J. Biochem. **138**, 729–739 (2005)
doi:10.1093/jb/mvi180

Interaction Analysis between tmRNA and SmpB from *Thermus thermophilus*

Nobukazu Nameki[1,2,*], Tatsuhiko Someya[1], Satoshi Okano[1], Reiko Suemasa[1], Michiko Kimoto[2], Kyoko Hanawa-Suetsugu[2], Takaho Terada[2], Mikako Shirouzu[2], Ichiro Hirao[2,3], Hiroshi Takaku[1], Hyouta Himeno[4], Akira Muto[4], Seiki Kuramitsu[2,5,6], Shigeyuki Yokoyama[2,5,7] and Gota Kawai[1,†]

[1]Department of Industrial Chemistry, Faculty of Engineering, Chiba Institute of Technology, Chiba 275-0016; [2]RIKEN Genomic Sciences Center, 1-7-22 Suehiro-cho, Tsurumi, Yokohama 230-0045; [3]Research Center for Advanced Science and Technology, The University of Tokyo, 4-6-1 Komaba, Meguro-ku, Tokyo 153-8904; [4]Department of Biochemistry and Biotechnology, Faculty of Agriculture and Life Science, Hirosaki University, Hirosaki 036-8561; [5]RIKEN Harima Institute at SPring-8, 1-1-1 Kouto, Mikazuki, Sayo, Hyogo 679-5148; [6]Department of Biology, Graduate School of Science, Osaka University, Toyonaka, Osaka 560-0043; and [7]Department of Biophysics and Biochemistry, Graduate School of Science, The University of Tokyo, 7-3-1 Hongo, Bunkyo-ku, Tokyo 113-0033

Received July 7, 2005; accepted September 5, 2005

Small protein B, SmpB, is a tmRNA-specific binding protein essential for *trans*-translation. We examined the interaction between SmpB and tmRNA from *Thermus thermophilus*, using biochemical and NMR methods. Chemical footprinting analyses using full-length tmRNA demonstrated that the sites protected upon SmpB binding are located exclusively in the tRNA-like domain (TLD) of tmRNA. To clarify the SmpB binding sites, we constructed several segments derived from TLD. Optical biosensor interaction analyses and melting profile analyses with mutational studies showed that SmpB efficiently binds to only a 30-nt segment that forms a stem and loop, with the 5′ and 3′ extensions composed of the D-loop and variable-loop analogues. The conserved sequences, 16UCGA and 319GAC, in the extensions are responsible for the SmpB binding. These results agree with the those visualized by the cocrystal structure of TLD and SmpB from *Aquifex aeolicus*. In addition, NMR chemical shift mapping analyses, using the 30-nt segment and ^{15}N-labeled SmpB, revealed the characteristic RNA binding mode. The hydrogen bond pattern around β2 changes, with the Gly in β2, which acts as a hinge, showing the largest chemical shift change. It appears that SmpB undergoes structural changes indicating an induced fit upon binding to the specific region of TLD.

Key words: induced fit, protein–RNA interactions, SmpB, tmRNA, tRNA-like domain.

Abbreviations: CMCT, 1-cyclohexyl-3-(2-morpholinoethyl) carbodiimide metho-*p*-toluene sulfonate; DMS, dimethylsulfate; EF-Tu, elongation factor Tu; OB-fold, oligonucleotide binding fold; tmRNA, transfer-messenger RNA; TLD, tRNA-like domain.

For quality control in protein synthesis, bacteria have a unique, elaborate translation mechanism, *trans*-translation, which is mediated by transfer-messenger RNA (tmRNA, also known as 10Sa RNA or SsrA RNA) that possesses both tRNA and mRNA properties. This RNA molecule is ubiquitous in the bacteria kingdom and has also been found in some chloroplasts and mitochondria (*1*, *2*). Various *in vivo* and *in vitro* experiments have supported the *trans*-translation scheme, as follows (for recent reviews, see Refs. *3* and *4*). The first step of the *trans*-translation reaction is the recognition by tmRNA of a stalled ribosome, which is caused, for example, by mRNA lacking a stop codon or possessing a cluster of rare codons. In the tRNA mode, a tmRNA charged with alanine by alanyl-tRNA synthetase enters the A-site of the ribosome via a ternary complex with EF-Tu and GTP, and donates the alanine to the growing polypeptide chain. In the next step, the tmRNA switches from the tRNA mode to the mRNA mode, and translation resumes at the first codon of the internal coding region of the tmRNA, followed by normal termination at the stop codon in the coding region. A tag peptide encoded by tmRNA is added to the C-terminus of the growing peptide, and the resultant tagged protein is immediately degraded by several tag-specific proteases. This process consequently promotes ribosome recycling and truncated mRNA degradation (*5*), and prevents the accumulation of abortively synthesized polypeptides during normal cell growth (*6*, *7*) and other biological events (*8–10*).

The function of tmRNA requires binding to several characteristic proteins. A unique basic small protein, SmpB, was first identified as an essential segment of the *trans*-translation system in *Escherichia coli* (*11*). This protein is found in all bacteria, and its sequence is relatively well conserved among them. Deletion of the *smpB* gene results in phenotypes similar to those observed in

*Present address: Department of Biological and Chemical Engineering, Faculty of Engineering, Gunma University, 1-5-1 Tenjin-cho, Kiryu-shi, Gunma 376-8515.
†To whom correspondence should be addressed. Tel: +81-474-78-0425, Fax: +81-474-78-0425, E-mail: gkawai@sea.it-chiba.ac.jp

tmRNA-defective cells, including a variety of phage development defects and a failure to tag proteins translated from defective mRNAs (*11*). In addition, purified SmpB binds specifically and with high affinity to tmRNA in a one to one ratio, and is required for the stable association of tmRNA with ribosomes *in vivo* (*12*). According to *in vitro* experiments using poly (U) dependent synthesis, SmpB binding to tmRNA enhances the aminoacylation of tmRNA, and meditates the ribosome binding of tmRNA, thus protecting it from degradation in the cell (*13*). In cells, this tmRNA-SmpB complex is included in a large ribonucleoprotein complex that comprises ribosomal protein S1, phosphoribosyl pyrophosphate synthase, RNase R, and a protein of unknown function encoded by the *yfbG* gene (*14*). A recent study indicated that ribosomal protein S1, which is known to bind to single-stranded RNAs, plays a role in delivering tmRNA to stalled ribosomes, although the protein is not ubiquitously present in bacteria (*15*, *16*). The three other proteins, however, do not appear to be essential for the *trans*-translation process itself, since efficient protein tagging occurs in a cell-free translation system lacking those (*17*).

Structural analyses of SmpB as well as tmRNA have facilitated remarkable advances in our understanding of the molecular mechanism of this unique process. The NMR structures of SmpB proteins from *Aquifex aeolicus* and *Thermus thermophilus* (~120 residues) revealed that the core of the protein consists of an antiparallel β-barrel twisted up from eight β-strands, which is capped with two α-helices (*18*, *19*). The core structure is followed by an unstructured region at the C-terminus (~20 residues), which always has an abundance of basic residues. Structural probing of the *E. coli* and *A. aeolicus* tmRNAs (~300 nt), in combination with extensive sequence alignments, indicated a characteristic tmRNA secondary structure, which appears to be common to many tmRNAs (*20*–*22*) (Fig. 1). The 5′ and 3′ termini form the tRNA-like domain (TLD), which has the acceptor stem with the 3′-CCA end, and the T-stem and loop as in canonical tRNAs, but lacks the D-stem. A pseudoknot structure (PK1), the internal coding region, and three pseudoknot structures (PK2-4) are sequentially arranged like a circle, and this region and the TLD are connected by a long stem including an internal loop (Helix 5, H5). Recently, the crystal structure of the TLD in a complex with SmpB from *A. aeolicus* revealed that TLD adopts an open, L-shaped conformation, and its elbow region is bound by SmpB (*23*).

In this study, we investigated the interaction of tmRNA with SmpB from *T. thermophilus*, from both the RNA and protein sides, by biochemical and NMR methods. First, we carried out a footprint procedure by chemical modification, to map the regions of full-length tmRNA that potentially interact with SmpB. To clarify which region is responsible for the SmpB binding, on the basis of the footprinting results, we constructed several RNA segments derived from the tmRNA secondary structure. Optical biosensor interaction analyses with mutational studies identified a 30-nt RNA segment that specifically binds to SmpB. NMR chemical shift mapping analyses of the RNA segment and SmpB revealed the characteristic interaction mode of tmRNA and SmpB. In addition, melting profile analyses showed the stable and specific interactions of SmpB with both the 30-nt RNA segment and tmRNA, which contribute to the thermal stabilization of the RNA structures. Furthermore, we found that significant structural changes in the protein structure are induced by the RNA binding.

MATERIALS AND METHODS

Protein Expression and Purification—Samples of SmpB from *T. thermophilus* were obtained using an *E. coli* expression system with chemically competent cells that contain extra copies of the *argU* and *proL* tRNA genes, to rescue the expression of genes restricted by the AGG/AGA and CCC codons. The expression and purification procedures were described previously (*19*).

Amplification of the tmRNA Gene from T. thermophilus *by PCR, Insertion into the pUC118 Vector, and* In Vitro *Transcription*—The DNA fragment containing the tmRNA gene was amplified, using the primers described below, from the genomic DNA of *T. thermophilus* HB8. The forward primer (5′-ATGTAATACGACTCACTATAgggggtgaaacggtctcgac-3′) contained a T7 promoter at its 5′ end, and the reverse primer (5′-GTGTGATGCAtggtggaggtgggggagtc-3′) contained an *Eco*T22I site at its 5′ end (lowercase letters indicate the tmRNA sequence). After phosphorylation of the 5′-termini of these primers, PCR amplification was performed with the phosphorylated primers and Pfu DNA polymerase (Promega, USA). The amplified DNA was directly ligated into the pUC118-*Hinc*II/BAP vector. The sequence of the insert was confirmed by sequencing. With this plasmid as the template, we performed PCR with the following primers, M4 (5′-GTTTTCCCAGTCACGAC-3′) and RV (5′-CAGGAAACAGCTATGAC-3′), and then digested the amplified DNA with *Eco*T22I to generate the tmRNA CCA end. Transcripts derived from the template DNA were prepared with a T7 run off-transcription system, using an AmpliScribe™ T7 Transcription Kit (Epicentre Technologies Co., USA). The transcripts were purified by electrophoresis on a 5% polyacrylamide gel containing 7 M urea. Transcripts of tmRNA from *E. coli* were prepared similarly.

Preparation of RNA Segments of tmRNA—Templates for *in vitro* transcription were constructed using two complementary synthetic DNA oligomers with a T7 promoter at the 5′ end. The forward and reverse oligomers were annealed, and transcripts were prepared as described above. The transcripts were purified by 12 or 15% polyacrylamide gel electrophoresis with 7 M urea. As for the T-arm (TD2), the corresponding RNAs were synthesized using an automatic DNA/RNA synthesizer, Expedite Model 8909 (PerSeptive Biosystems, Inc., USA), and were purified as described (*24*).

Chemical Probing and Footprinting Experiments Using the Primer Extension Method—DMS and CMCT (Nacalai Tesque, Japan) were used for chemical modification. The reaction conditions were basically those previously described (*21*). Prior to chemical modification, the RNA (0.25 μM) was heated at 97°C for 30 s, and then was cooled slowly to 20°C in the reaction buffer as described below. After the addition of SmpB (1.0 μM, final concentration), the mixtures were incubated at 75°C for 10 min, and then were cooled slowly to 50°C.

In the case of the CMCT modification, a 60 μl aliquot of the RNA-SmpB complex solution, in buffer A [50 mM

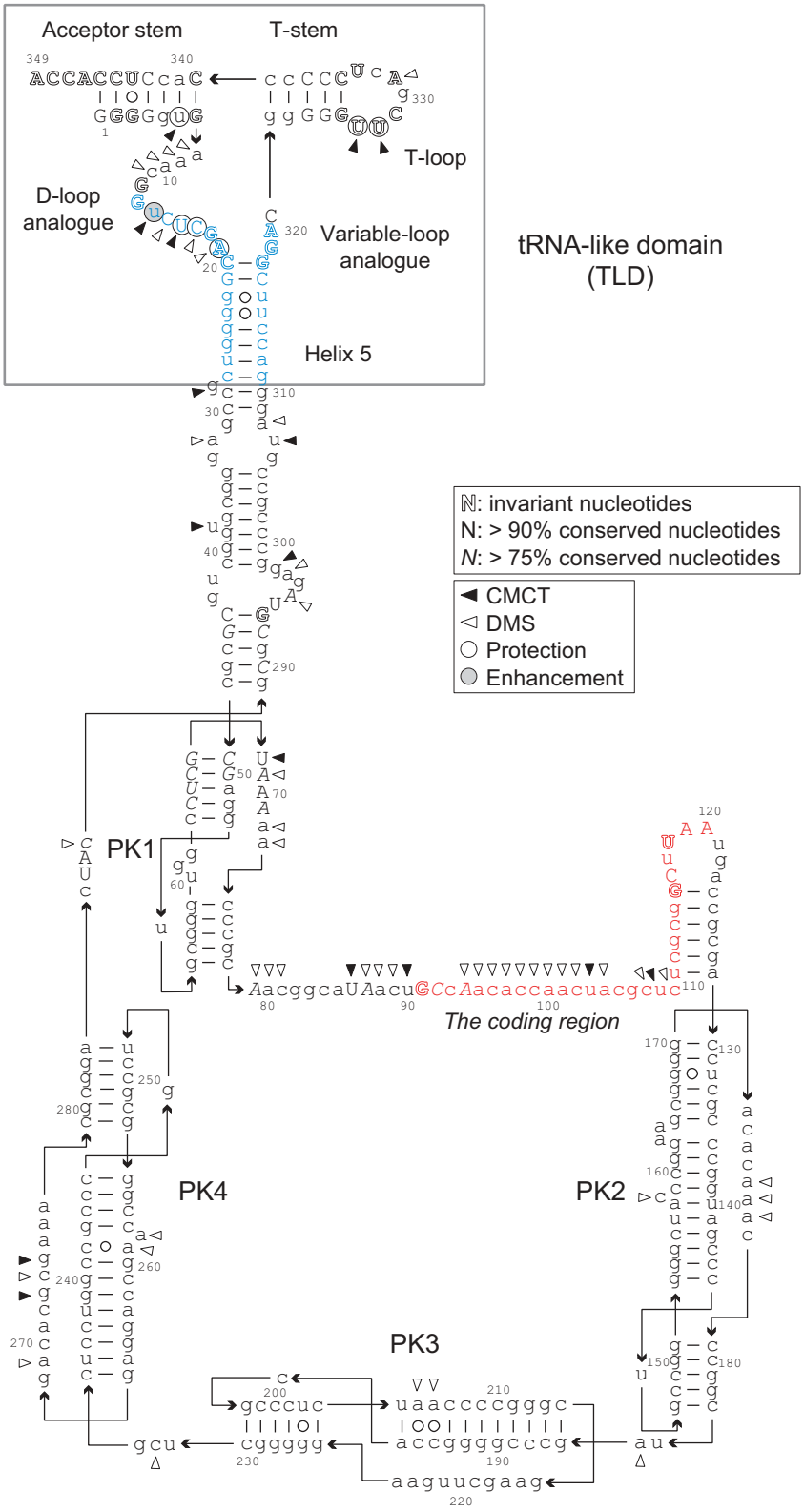

Fig. 1. **Secondary structure diagram of tmRNA from *T. thermophilus* showing the results of the footprinting analysis.** The sequence is cited from Bekke *et al*. (*44*), except for the nucleotide at position 310 (A310), which is different from that obtained in this study (G310). The tRNA-like domain (TLD) is boxed. The region corresponding to the TD3 segment and the coding region are shown in blue and red, respectively. According to the comparative sequence analysis by Zwieb *et al*. (*22*), outlined letters indicate invariant nucleotides among the species. Upper-case letters mark residues that are >90% conserved; upper case and italicized letters indicate >75% conservation. The stem numbering is also according to Zwieb *et al*. (*22*). In the footprinting analysis, nucleotides modified by CMCT and DMS in the absence of SmpB are indicated by filled and empty triangles, respectively. Nucleotides protected from chemical modifications upon SmpB binding are encircled, and those in which an enhancement in the activity occurs are denoted by hatched circles. As for the second loop of PK3, all of the positions were so easily cleaved in the free tmRNA that we could not detect chemical modifications in the region.

sodium borate (pH 7.9), 20 mM magnesium acetate], was mixed with 60 μl of CMCT (42 mg/ml in buffer A) followed by incubation at 50°C for 30 min. In the case of the DMS modification, a 60 μl aliquot of the RNA-SmpB complex solution in buffer B [50 mM sodium cacodylate (pH 7.4), 20 mM magnesium acetate] was mixed with 3 μl of DMS (diluted 15-fold in ethanol) followed by incubation at 50°C for 10 min.

The reaction was stopped by the addition of 1/10 volume of 3 M sodium acetate (pH 5.4) and 2.5 volume of ethanol. After resuspending the pellet in 200 μl of 300 mM sodium acetate, the modified RNAs were extracted with phenol and chloroform, and then were precipitated with ethanol. The collected RNAs were dissolved in 30 μl of distilled water.

Primer extension was performed with reverse transcriptase (RAV-2) and oligonucleotide primers labeled at the 5′-end with [γ-^{32}P]ATP and T4 polynucleotide kinase. The oligonucleotide primers used were complementary to residues G31–C49 (P1), C84–C105 (P2), C116–C133 (P3), G152–G170 (P4), G186–C203 (P5), C209–G225 (P6), A258–G275 (P7), G303–A320 (P8), and U333–A349 (P9). Modified sites were indirectly detected by gel electrophoresis, by analyzing the DNA sequence patterns generated through primer extension upon reverse transcription of the modified RNAs.

Optical Biosensor Assay for Interaction between SmpB and RNAs—We used an IAsys™ instrument and CM Dextran cuvettes from Affinity Sensors, UK. The SmpB protein was placed in a cuvette for 7 min at a final concentration of 0.25 mg/ml in a final volume of 100 μl, and was covalently immobilized following the protocol provided by Affinity Sensors. In a typical experiment, RNAs were added at different concentrations in 100 μl of buffer, containing 20 mM sodium phosphate buffer (pH 6.5), 100 mM sodium chloride and 1 mM magnesium chloride, and the increase in arc seconds was measured versus time at 25°C. The bound RNAs were removed by incubation for 2 min in 1.5 M sodium chloride. Repeated washes with 1.5 M sodium chloride did not affect the RNA binding capacity of SmpB. Curves were fitted using the FASTfit™ software package from Affinity Sensors. A single exponential function was used to fit the individual binding curves, to obtain the pseudo first-order rate constants in units of s^{-1} for each RNA concentration (*25*). The association rate constant, k_{ass}, was derived from the gradient of the plot of the first-order rate constant against the RNA concentrations. The dissociation rate constant, k_{diss}, was derived directly from the time course of dissociation. The dissociation constant, K_d, was then calculated as the ratio of k_{diss}/k_{ass}.

Melting Profiles of Transcripts—The absorbance at 260 nm and the melting temperatures were monitored with a spectrophotometer (DU-640; Beckman, USA) equipped with a temperature regulator and a six-cell holder. Before the measurements of the melting temperatures, the RNAs (~0.16 μM) were heated to 90°C for 3 min in the absence of both monovalent and divalent cations, and then were chilled quickly on ice. The measurements were made using the same buffer conditions as those used in the optical biosensor assay.

Titration by NMR—Samples of ^{15}N-labeled SmpB from *T. thermophilus* were also obtained in the *E. coli* expression system, as described (*19*). The protein concentration was ~0.1 mM in $^{1}H_2O/^{2}H_2O$ (9:1) sodium phosphate buffer (pH 6.0) containing 150 mM sodium chloride. Before the protein and RNA were mixed, each sample was independently incubated at 60°C for 10 min. After the TD3 RNA sample in the same buffer had been added to the NMR tube containing 400 μl of the SmpB protein, the mixed sample in the tube was equilibrated at 60°C for 10 min before the NMR measurements. The RNA was introduced in four steps, at molar ratios (RNA:SmpB) of 0, 0.5, 1.0 and 1.3. Measurements of ^{15}N-^{1}H HSQC spectra were performed at 45°C on Bruker DRX-600 spectrometers. The backbone assignments at pH 4.0 had been determined previously (*19*), and we performed the pH titration experiments from pH 4.0 to pH 6.0 to determine the backbone assignments at pH 6.0 (data not shown). Changes in average amide chemical shifts were calculated using $\Delta\delta av = \{0.5\ [(0.2\ \Delta\delta N)^2 + \Delta\delta H^2]\}^{1/2}$, where $\Delta\delta N$ and $\Delta\delta H$ are the amide nitrogen and amide proton chemical shift differences between the free and the bound states of the protein.

The spectra were processed using the program NMRPipe (*26*), and were visualized and analyzed using the program Sparky (*27*). The program MOLMOL (*28*) was used to analyze the various structures and to prepare the figures.

RESULTS AND DISCUSSION

Chemical Footprinting Analyses to Determine the SmpB Binding Site in the Full-Length tmRNA—We performed chemical footprinting analysis to delineate the region of tmRNA that was protected by *T. thermophilus* SmpB. The full-length tmRNA transcript was incubated at 75°C, either without or with SmpB, and then was subjected to modification by DMS (to probe A at N-1, and probe C at N-3) and CMCT (to probe U at N-3 and weakly probe G at N-1) at 75°C for 10 min. Both reagents are reactive only with unpaired nucleotides in footprinting experiments. Reactive positions were identified by primer extension analyses (Fig. 2).

The results are summarized in Fig. 1. In the case of the free tmRNA, the positions that reacted with the two chemical probes were mapped in most of the unpaired regions in the secondary structure model: the D-loop analogues of TLD, the loops in the linker region, the coding region, and the longer loops of all of the pseudoknots. This chemical probing pattern is consistent with the secondary structure diagram of *T. thermophilus* tmRNA (Fig. 1), which was derived from extensive sequence alignments with chemical probing analyses in *E. coli* (*20–22*). The results show that the folding of this tmRNA transcript is virtually identical to that of the native tmRNA.

Changes in the local environments of residues were mapped by comparing the DMS and CMCT reactivities of the free tmRNA with those of the tmRNA-SmpB complex. Upon SmpB binding, only the TLD region became protected from the chemical modifications, whereas no significant footprints were observed in the other regions (Fig. 1). These results demonstrate that TLD is the major binding site for SmpB. Protected sites were located at positions U16, C17 and A19 in the D-loop, U327 and U328 in the T-loop, and U6 in the acceptor stem. An enhancement in the reactivity occurred only at U14 in the D-loop, which was located close to the protected region from U16 to A19. It is notable that all of the nucleotides, except for U6, are highly conserved among all of the known tmRNAs (Fig. 1). These results agree well with those obtained in enzymatic (RNases S1 and V1) and chemical (lead acetate) footprinting analyses, using the TLD of tmRNA and SmpB from *A. aeolicus*. In footprinting experiments, generally, the protection from chemical modification is due to direct interactions of a protein with the protected nucleotides, and/or protein-induced structural

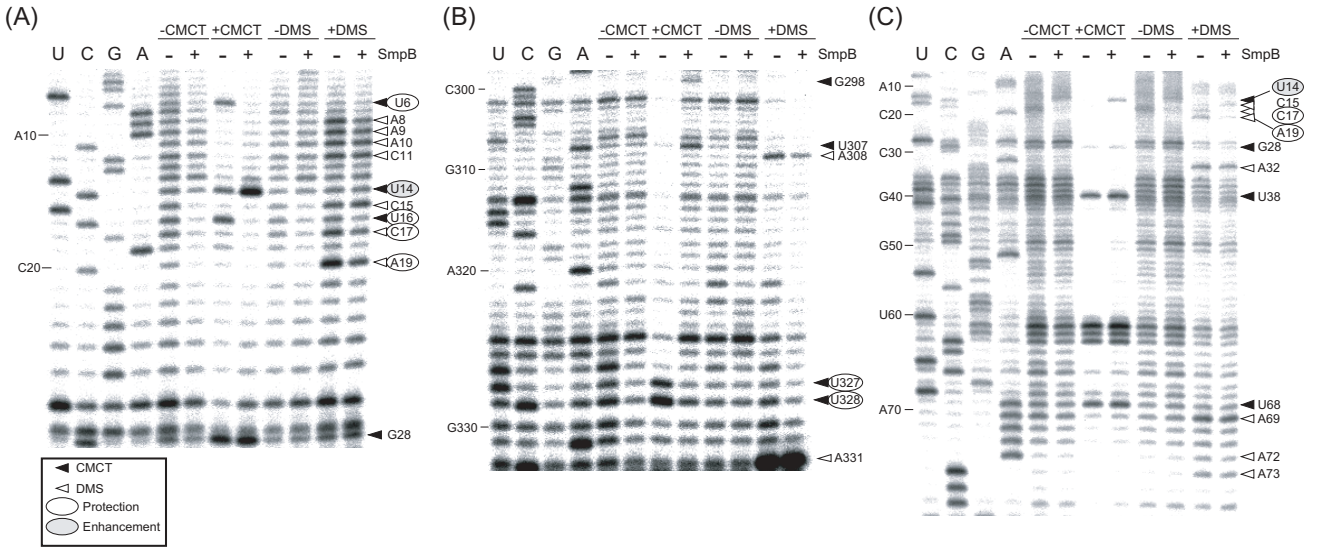

Fig. 2. **Primer extension analysis of chemical modifications of the full-length tmRNA.** Shown are mapping data with and without CMCT and DMS treatments in the absence (–) and presence (+) of SmpB, using primer P1 (A), primer P9 (B), and primer P2 (C). The sequenced regions in (A) and (B) mainly include TLD, and those in (c) include the PK1 region. Lanes A, G, C, and U are sequencing ladders generated in the presence of ddTTP, ddCTP, ddGTP, and ddATP, respectively. The symbols are the same as those in Fig. 1.

Table 1. **Kinetic parameters of tmRNA and its segments for binding SmpB from *T. thermophilus*.**

Ligands	k_{ass} (M^{-1} s^{-1})	k_{diss} (s^{-1})	K_d (M)	Relative K_d
Full-length tmRNA	$2.0 \pm 0.4 \times 10^{5}$	$4.1 \pm 0.6 \times 10^{-3}$	$2.1 \pm 0.7 \times 10^{-8}$	1
TD1 (the acceptor arm)			$>2.0 \times 10^{-5}$	>1,000
TD2 (T-arm)			$>2.0 \times 10^{-5}$	>1,000
TD3	$2.2 \pm 0.2 \times 10^{4}$	$1.4 \pm 0.3 \times 10^{-2}$	$6.5 \pm 1.5 \times 10^{-7}$	32
TD3a	$6.7 \pm 0.3 \times 10^{4}$	$2.2 \pm 0.5 \times 10^{-2}$	$3.3 \pm 0.9 \times 10^{-7}$	16
TD3b			$>2.0 \times 10^{-5}$	>1,000
TD3c			$>2.0 \times 10^{-5}$	>1,000
TD3d	$2.8 \pm 0.6 \times 10^{3}$	$1.1 \pm 0.1 \times 10^{-2}$	$3.9 \pm 1.4 \times 10^{-6}$	190
TD3e			$>2.0 \times 10^{-5}$	>1,000
TD4 (H5 stem)			$>2.0 \times 10^{-5}$	>1,000

changes in the RNA structure. An expanded discussion of the SmpB binding to TLD will be presented later, in view of the RNA structural changes.

Optical Biosensor Interaction Analysis Showing the Binding Nucleotides in TLD—To analyze the kinetics of the RNA-protein interaction, we performed an optical biosensor assay with an IAsys™ instrument, based on the resonant mirror device (Affinity Sensors, UK) (*29*). RNA binding was monitored in real time, by the change in the density of the protein-coated sensor surface. The accumulation of mass within the optical window at the sensor surface affects the angle of light reflection, and this angle was measured. The association and dissociation phases of the sensorgrams for a series of RNA concentrations were analyzed to determine k_{ass} and k_{diss}, as described (*25*, *30*), where k_{ass} and k_{diss} are the association and dissociation rate constants, respectively. Kinetic analyses showed that SmpB from *T. thermophilus* binds to the full-length tmRNA transcript from *T. thermophilus*, with a k_{ass} of 2.0×10^{5} M^{-1} s^{-1}, a k_{diss} of 4.1×10^{-3} s^{-1}, and thus a K_d of 21 nM (Table 1). In addition, SmpB was also shown to bind to the tmRNA transcript from *E. coli* with similar affinity (data not shown). The K_d value agrees well with that obtained from the *E. coli* system, as estimated by RNA gel mobility shift assays (~20 nM), confirming that the T7 transcripts and the purified SmpB overexpressed in *E. coli* were functional for the footprinting and optical biosensor experiments.

To clarify which region is responsible for the SmpB binding within TLD, we used the basis of the footprinting results to guide the construction of four RNA segments derived from the secondary structure of TLD (Fig. 3). The four segments are: TD1, the acceptor arm containing the acceptor stem and the T-arm; TD2, the T-arm; TD3, a stem that is part of the H5 stem and is closed by a UUCG loop, with the 5′ and 3′ extensions composed of the D-loop and variable-loop analogues that are well protected in the footprinting analysis; and TD4, the H5 stem including an internal loop closed by a UUCG loop. The optical biosensor interaction analysis showed that whereas SmpB does not efficiently bind to TD1, TD2, or TD4, it binds to TD3 with a K_d of 0.65 μM, resulting in a 32-fold increase in the K_d, as compared to that of tmRNA (Table 1). Furthermore, to verify whether SmpB binds to TD3 *via* the protected

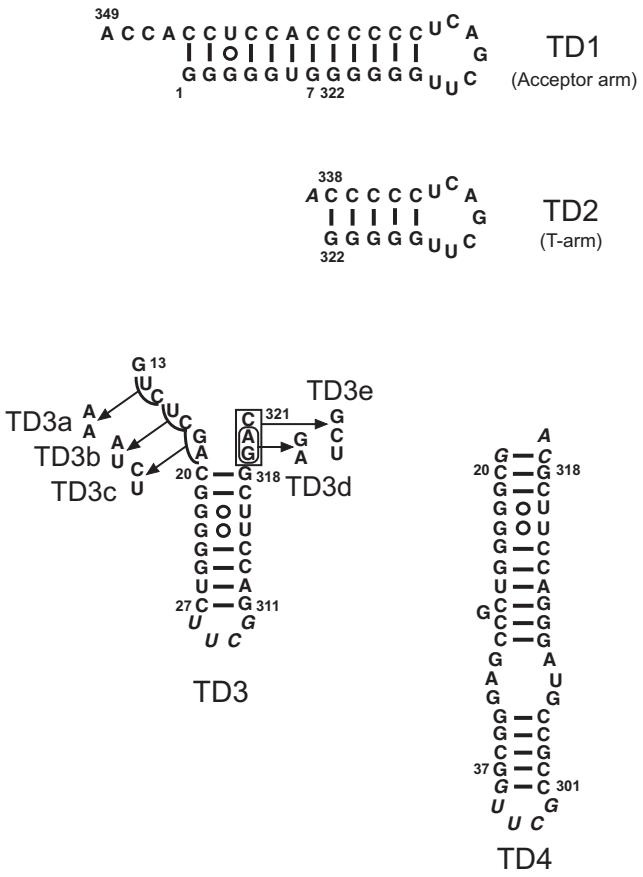

Fig. 3. **Representations of the secondary structures of the segments derived from TLD.** Italicized letters indicate the nucleotides that are not original. In TD3 and TD4, a stable UUCG tetraloop (shown in italics) is used to close a helix. In TD3, arrows indicate the nucleotide changes with the mutant names. The numbering of the segments is according to that of the full-length tmRNA from *T. thermophilus*.

nucleotides in the extensions, we introduced various mutations into the extension regions (Fig. 3). For the 5′ extension region, the change from 14UC to AA (TD1a) had no effect on the binding affinity to SmpB, whereas the changes from 16UC to AU (TD1b) and from 18GA to CU (TD1c) severely affected the binding affinity to SmpB (Table 1). In addition, when the 13GUCUC nucleotides were deleted and a G-C pair was added to close the stem ending in the conserved GA and AG sequences, the resulting mutant, which forms a normal helix, lost its binding affinity to SmpB. For the 3′ extension region, the change from 319GA to AG (TD3d) resulted in a 6-fold increase in the K_d as compared to that of TD3, and a significant decrease in the binding affinity was observed in the mutant with the change from 319GAC to UCG, which creates three Watson-Crick pairs between the 5′ and 3′ extensions (TD1e). These findings indicate that the SmpB binding to TD3 requires the highly conserved nucleotides of the D-loop and the variable-loop analogues, 16UCGA and 319GAC. These findings agree well with those obtained from the crystal structure of TLD SmpB from *A. aeolicus*, in which these nucleotides directly interact with the conserved residues of SmpB (*23*). It thus appears that SmpB binds to the 30-nt segment, TD3, in a similar manner as to the tmRNA composed of 349 nucleotides. In *E. coli*, it has been shown that the regions in *E. coli* tmRNA corresponding to the 16UCGA and 319GAC regions in *T. thermophilus* tmRNA are important for *trans*-translation, rather than aminoacylation (*31*), and particularly, G18 and A320 (G19 and A334 in *E. coli*, respectively) are the key nucleotides involved in several SmpB functions (*13*).

Melting Profile Analysis Showing the Contribution of SmpB Binding to the Thermal Stability of the tmRNA Structure—Protein binding to DNA/RNA often increases the melting temperature (T_m) of DNA/RNA. We first examined whether the SmpB binding stabilizes the tmRNA structure. First derivative plots of the melting are shown in Fig. 4. The largest peak appeared at 73.1°C,

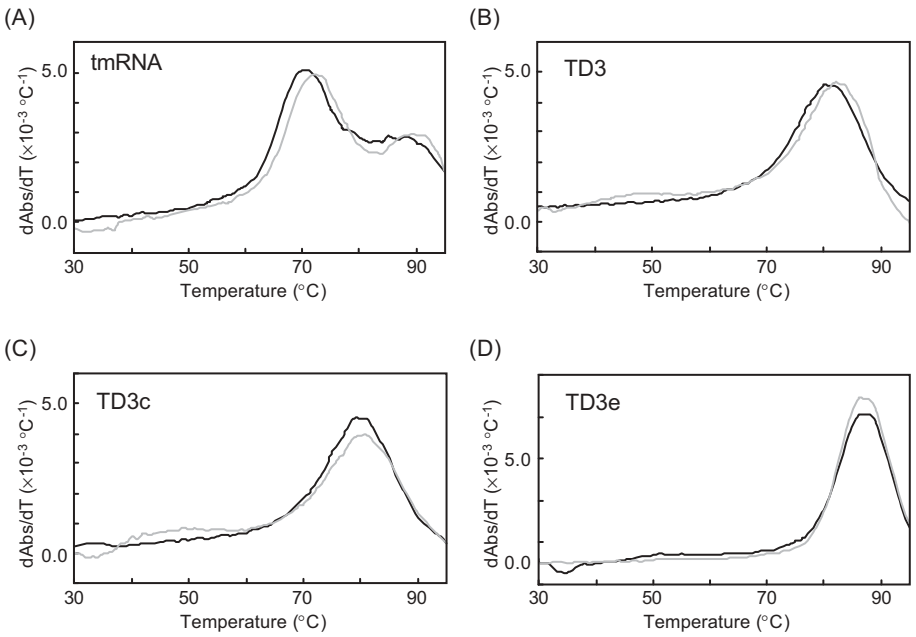

Fig. 4. **First derivative plots of UV melting curves of tmRNA (A), TD3 (B), and the TD3 mutants, TD3c (C) and TD3e (D).** The plots of TD3a, TD3b and TD3d are not shown, because they are essentially the same as the plot of TD3 or TD3c (see text). As for TD3e, the T_m value is larger than that of any other mutant, because the number of base pairs is larger by three.

Table 2. **Melting temperatures of the TD3 segment, and its mutants, in the presence and absence of SmpB from *T. thermophilus*.**

	T_m (°C)	
	without SmpB	with SmpB
tmRNA*	73.1	75.2
TD3	80.2	82.2
TD3a	80.8	82.4
TD3b	81.7	81.4
TD3c	80.2	80.2
TD3d	81.5	81.1
TD3e	87.1	87.4

*For tmRNA, only the T_m value of the largest peak is given.

followed by a second broad peak. The addition of SmpB shifted the whole plot profile by about 2°C (Table 2). These results show the stable and specific interactions between SmpB and tmRNA that contribute to the thermal stabilization of the tmRNA structure.

To verify the specificity of SmpB binding to TD3, we measured the thermal melting profiles of TD3 and its mutants in the absence and presence of SmpB. Comparisons of the first derivative plots of TD3 in the absence and presence of SmpB showed a 2°C shift of the plot profile. For the mutants, a similar result was observed in only TD3a, whereas none of the other mutants had any effects on the T_m values, although the profiles were somewhat altered (Table 2). These results are consistent with those obtained by the biosensor analysis, which showed that SmpB binds to TD3 *via* the extension sequences, thermally stabilizing the RNA structure.

NMR Chemical Shift Mapping to Reveal the Structural Changes of SmpB Induced by the RNA Binding—To investigate how *T. thermophilus* SmpB interacts with TD3, we performed NMR chemical shift perturbation experiments. We have previously determined the NMR structure of *T. thermophilus* SmpB. Samples of the ^{15}N-labeled SmpB were mixed with TD3 at 60°C, and ^{1}H-^{15}N HSQC spectra were acquired at 45°C to monitor the chemical shift changes in the backbone amides induced by the RNA binding. A comparison of the spectra without and with the RNA showed a number of differences in the peaks, including chemical shift changes and peak broadening or disappearance (Fig. 5), indicating specific interactions between TD3 and SmpB. Peak broadening and disappearance are often observed in RNA-protein interaction experiments, making peak monitoring difficult. This would be partly caused by an exchange rate between the free and bound states on an intermediate time scale; in fact, the K_d value of TD3 is 0.65 μM, and thus the RNA–protein interaction is not so tight.

Figure 6 shows the chemical shift mapping on the SmpB structure, where chemical shift changes were observed all over the structure. The cocrystal structure of TLD and SmpB from *A. aeolicus* allowed us to determine whether the chemical shift changes are fundamentally due to direct interactions with the protein or to indirect structural changes induced by the RNA binding. In view of this, the chemical shift changes are useful as sensitive markers indicating structural differences between free and bound SmpB. Among the residues showing significant chemical shift changes, Glu21, Gly23, Ala25, Lys27, Glu49, Gly51,

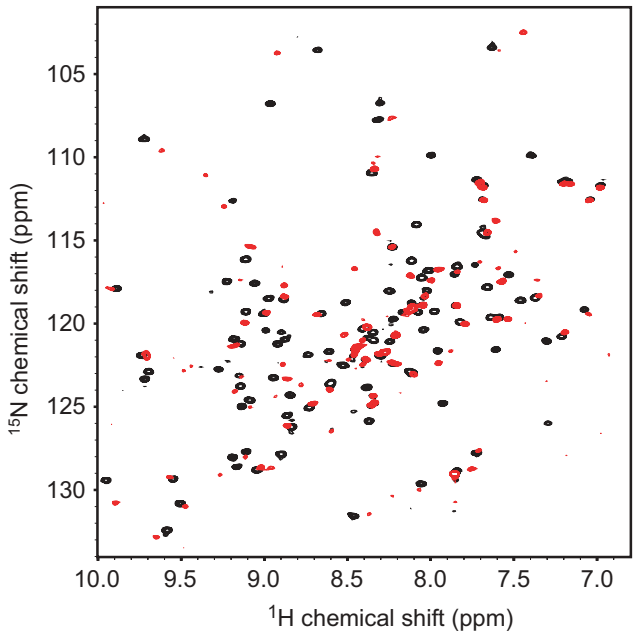

Fig. 5. **Superposition of the ^{1}H-^{15}N HSQC spectra of free 15N-labeled SmpB (black) and that in a complex with TD3 (red) in a one to one ratio.**

Lys78, and Gly111 are located on the surface interacting with the RNA, whereas the other residues are obviously far from the interacting surface (Fig. 6). These results suggest that SmpB undergoes extensive structural changes induced by the RNA binding. This is supported by a comparison of the free and bound forms of SmpB from *A. aeolicus*, which revealed remarkable structural changes within the entire structure, including a shift of the β-barrel conformation in the bound state to a more twisted form than in the free state (Fig. 7A). Hence, these structural changes lead to the wide distribution of the chemical shift changes. This is the first report indicating that significant structural changes of SmpB are induced by RNA binding. Note that the numbering of SmpB and tmRNA from *E. coli* and *A. aeolicus* in this paper is according to that for *T. thermophilus*.

The chemical shift changes of a few conserved residues highlight the characteristic features of the structural changes in SmpB. The largest chemical shift change was observed in Gly23 in β2, and the neighboring residue, Ala22, also shows a significant change (Table 3). It appears that these changes are involved in the alteration of the hydrogen bond pattern of the β-sheet, with the two small residues acting as a hinge (Fig. 7B). In the absence of the RNA, the Ala22 and Gly23 residues are included in β2, with the HN of Ala22 hydrogen-bonding with the O of Val120 in β6. In the presence of the RNA, according to the crystal structure, the ϕ and ψ angles of Ala22 drastically changed, by about +110° and +67° (–113° → –5°; 165° → –136°), respectively, while the ϕ angle, but not the ψ angle, of Gly23 changed by about –20° (–123° → 102°; 101° → 99°). It is notable that the angles of the other residues in β2 and β6 hardly changed upon RNA binding. Consequently, the two hydrogen bonds between β2 and β6 (the HN of Ile29–the O of Val118, and the O of Ala27–the HN of Val120) are

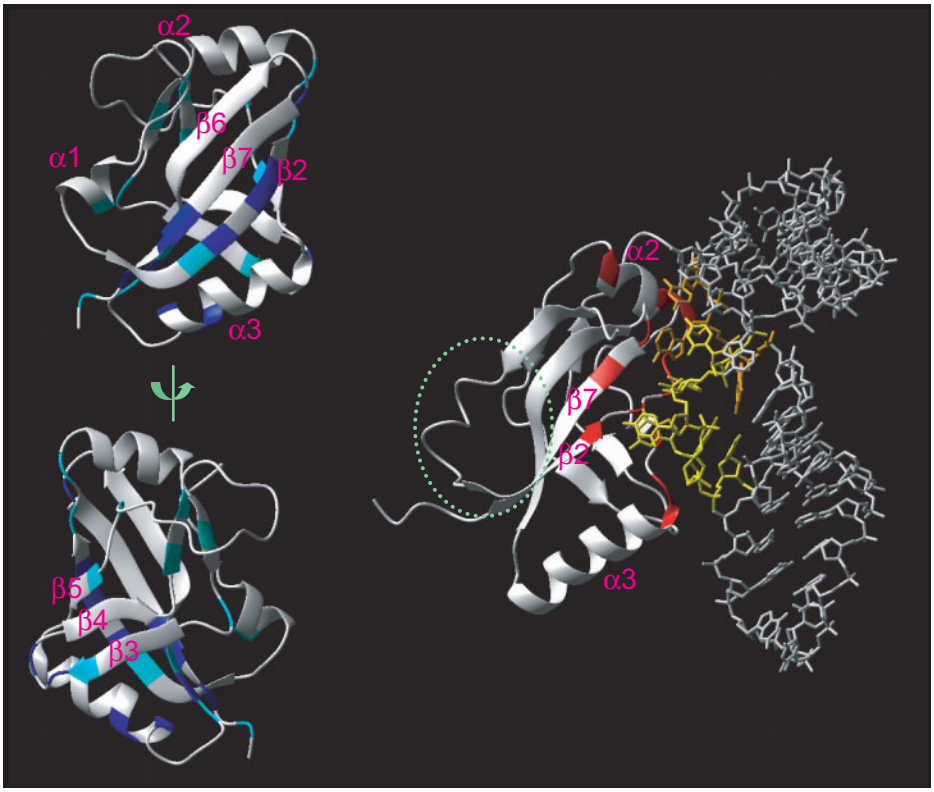

Fig. 6. **Chemical shift mapping of SmpB with TD3, indicating structural changes all over the protein structure.** Ribbon representations of *T. thermophilus* SmpB (PDB code 1J1H) (top and bottom left), and that of *A. aeolicus* SmpB in a complex with TLD (1P6V) (right). The residues colored blue and light blue represent those that exhibited a normalized weighted average of the chemical shift difference (Δδav) of the amide groups greater than 0.2 and 0.1 ppm, respectively. On the right, the colored residues (red) and nucleotides (16UCGA, yellow and 319GAC, orange) indicate direct interaction sites, as described (*23*). Another potential RNA-binding region is indicated by a green circle, as described in the text.

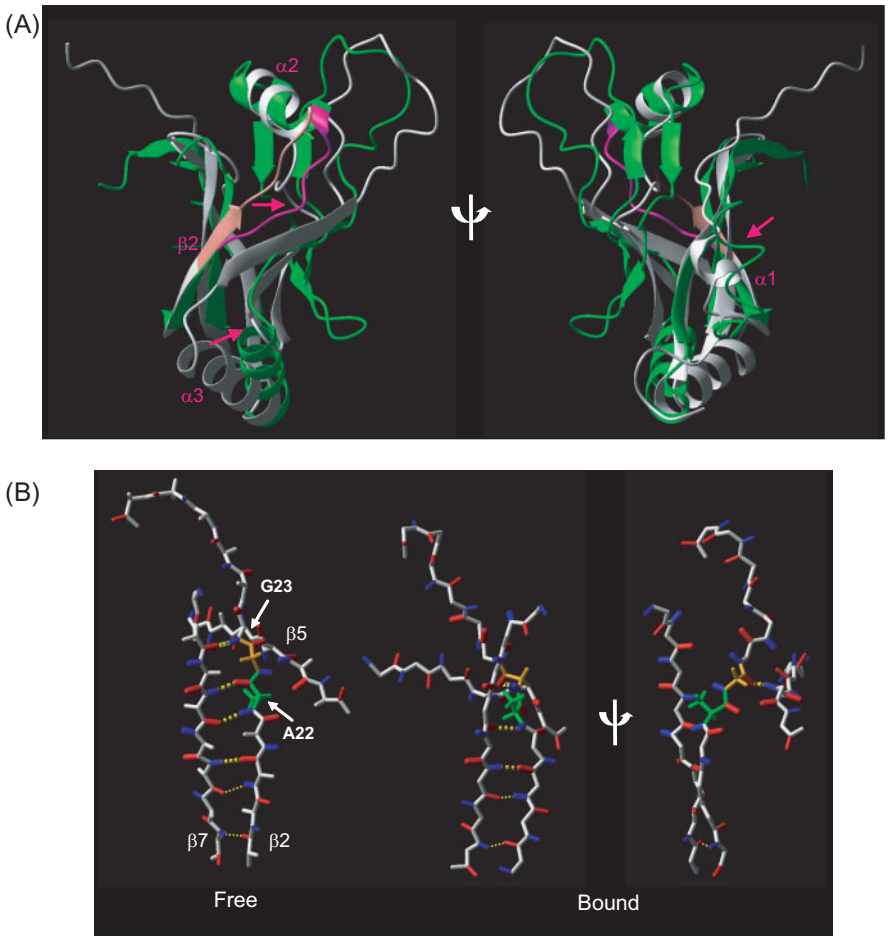

Fig. 7. **Structural comparison of free and bound SmpB.** (A) Superimposition of the free (white) and bound (green) forms of SmpB from *A. aeolicus* (PDB codes 1K8H and 1P6V). The region corresponding to the highly conserved sequence of ^{21}EAG(I/L)xLxGxE(I/L)K^{32}, which involves the alteration of the hydrogen bond, as described in text, is shown in pink (free) and magenta (bound). (B) Alteration of the hydrogen bond pattern in the center of Gly22 and Ala23 in β2, as shown in (A). The HN bonds and the CO bonds are shown in red and blue, respectively, and the two residues, including their side chains, are shown in green. Hydrogen bonds are depicted by yellow dotted lines.

Table 3. **Chemical shift differences for the backbone amides in the complex with TD3, using the normalized weighted average chemical shift differences of the backbone amide ^{1}H and ^{15}N resonances.**

Res.	Location	Δδav	Res.	Location	Δδav
N7	α1	0.08	L55	β4	0.05
A10	α1	0.12	E56	β4	0.09
R11	α1	0.08	N57		0.03
H12	α1	0.09	**Y59**	β4′	0.16
D13		0.07	I60	β4′	0.06
Y14		0.07	A61	β4′	0.16
E15		0.09	A69		0.04
I16	β2	0.04	V71		0.01
L17	β2	0.05	D72		0.06
T19	β2	0.11	R74		0.03
Y20	β2	0.36	R75		0.12
E21*	β2	0.05	**K78**	β5	0.15
A22*	β2	0.49	H82*		0.08
G23*	β2	2.35	R87	α3	0.05
A25*		0.11	**G91**	α3	0.46
K27*		0.18	K92	α3	0.06
K32	α2	0.07	V93	α3	0.33
G37		0.08	**L98**		0.11
K38	β3′	0.06	**T99**	β6	0.34
V39	β3′	0.18	**L100**	β6	0.11
F41		0.04	V101	β6	0.03
T42		0.11	**G111***		0.38
S44		0.00	**L117**	β7	0.62
A46	β3	0.09	G118	β7	0.31
F48	β3	0.15	L119	β7	0.08
E49*		0.46	**A120**	β7	0.20
G51*		0.26	**G122**		0.15

Changes in average amide chemical shifts were calculated using $\Delta\delta av = \{0.5\ [(0.2\ \Delta\delta N)^2 + \Delta\delta H^2]\}^{1/2}$, where ΔδN and ΔδH are the amide nitrogen and amide proton chemical shift differences between the free and the bound states of the protein. Residues in bold indicate changes larger than 0.1 ppm, and they are shown in the SmpB structure in Fig. 6. Asterisks indicate the residues located on the interacting surface.

disrupted, and instead the O of Gly28 hydrogen-bonds with the HN of Leu86 in the neighboring strand β6 followed by α3 (Fig. 7B). This alteration of the hydrogen bond pattern allows the space between α2 and the β-sheet, formed by β2-β6-β5, to expand, relative to that of the free SmpB, so the space can accommodate the interacting nucleotides of TLD (Fig. 7A). Interestingly, the Gly and Ala residues in β2 are highly conserved. This alteration mechanism, in which the angle alteration requires such a small residue, seems to have been conserved in the SmpB–TLD interaction.

Other significant changes are clustered in a region, exactly opposite from the direct interaction site, that includes the first half of β5 (Leu98, Thr99, and Leu100), the latter half of β6 (Leu117, Gly118, Ala120, and Gly122), the N-terminal end of α3 (Gly91 and Val93), and α1 (Ala10) (Fig. 6). A comparison between the free and bound SmpB structures shows that these regions exhibit apparent differences (Fig. 7A). Particularly, the direction of α2 is different, and the pitch of α1 is changed such that α1 becomes a coil, rather than an α-helix. Thus, these structural changes result in the chemical shift changes. Interestingly, around this region a second potential RNA-binding site involved in the ribosome binding is formed when the tmRNA-SmpB complex enters the ribosome (Fig. 6, right) (*18*). Such a local structural change may be necessary to permit other SmpB functions in the stages after the tmRNA binding.

Structural Changes in the RNA as Well as the Protein—The structural changes of SmpB accompany those of the RNA structure of TLD. In unbound tmRNA, some experimental results indicated that TLD has some tertiary interactions, like an L-shaped conformation between the D-loop analog and the T-loop (*32*, *33*), with an internal angle of 110° (*34*). A 2D NMR analysis supports the existence of the tertiary interaction that is mediated by the base-pairing between 328UC in the D-loop and 12GG in the D-loop analogue, as seen in canonical tRNAs (*35*). However, the TLD structure in complex with SmpB appears to have no such interactions, although the 12 nucleotides ranging from G1 to G12 are not observed. Particularly, U328 is located inside the T-loop, and is stacked with U327, and thus it could hardly interact with 12GG because of the long distance between them, even if its base could move freely. The TLD structural changes have been supported by a few footprinting experiments, including those in this study. The region around the conserved 327UUC region in the T-loop displays some differences in the footprint patterns between in the absence and presence of SmpB, although the region is not bound by SmpB (*23*, *36*). It should be noted that in native *E. coli* tmRNA, U327 and U328 in the T-loop are modified to 5-methyluridine (m^5U) and pseudouridine (ψ), respectively, although it is unknown whether the modifications are essential for the tertiary interaction (*37*). These findings suggest that SmpB binding leads to structural changes or rearrangement of the TLD elbow region. One scenario involves SmpB efficiently recognizing such a preformed, L-shaped tmRNA structure, followed by structural changes of both the protein and RNA to form the functional complex. This process would involve an induced fit that mediates the control of specificity and biological function, as often seen in RNA-protein interactions (*38*, *39*).

Recently, visualization of tmRNA entry into a stalled ribosome has been reported by a cryo-electron microscopy (cryo-EM) study of the SmpB-TLD complex with EF-Tu in the kirromycin-stalled ribosome (*40*). Intriguingly, it was pointed out that the binding mode of SmpB and TLD on the ribosome apparently differs from that off the ribosome, in terms of the orientation of the SmpB and the H5 stem (*23*, *40*). This difference implies further structural changes of the complex on the ribosome.

The Unique Binding Mode of an Extended OB Fold—SmpB consists of an antiparallel β-barrel formed from eight twisted β-strands (Fig. 6). It was thought that an OB-fold, composed of a five-stranded β-barrel, is embedded in the β-barrel structure of SmpB (*18*), and thus the unique fold of SmpB was termed an extended OB-fold (*19*). The RNA interaction mode, however, significantly differs between the two folds (Fig. 8). The majority of OB-fold proteins use the same face of the β-sheet for ligand binding, which is centered on β2 and β3 (*41*). In contrast, SmpB mainly uses the regions connecting the β-strands, rather than a β-sheet face: β2 and β3; β5 and β6; and β6 and β7. Particularly, the RNA contact area of the β2/β3 region, ranging from the end of β2 through the first half of α2, is the largest among the three, and is occupied by

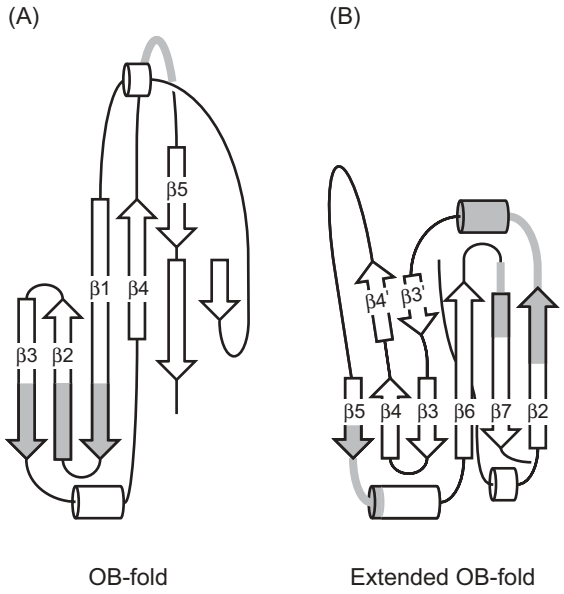

Fig. 8. **Comparison of the secondary structure diagrams of the OB fold (aspartyl-tRNA synthetase) and the extended OB fold (SmpB).** The RNA interaction sites are shown in gray.

the highly conserved sequence of ^{21}EAG(I/L)xLxGxE(I/L/V)K^{32}, which is involved in the alteration of the hydrogen bond, as described above. The region enters the major groove of the RNA, and participates in base-specific interactions with TLD. It is important to note that this region corresponds to that which is supposed to be added to the typical OB-fold. Among the RNA/DNA binding proteins examined thus far, this binding mode, in which the β-strands do not play major roles in the interactions, is unique to SmpB, and seems to have become specialized for tmRNA binding throughout evolution. On the other hand, as described above, SmpB has another potential RNA-binding site. If so, it would be interesting to determine whether the β-sheet is used for an OB-fold type of RNA interaction.

Concluding Remarks—In addition to the structural core region that has been discussed thus far, SmpB always has a poorly ordered, basic-rich region (~15 residues) at the C-terminus, followed by β6, including the highly conserved sequence of ^{123}KKxx(D/E)KR^{129}. Considering the abundance of basic residues, it is thought that this region interacts with RNA within the ribosome, and becomes structured, as seen in some ribosomal proteins (*42*). Recent experiments using SmpB from a diatom species, with a plastidial tmRNA and the *smpB* gene encoded in the nucleus, revealed that the SmpB protein is active for *trans*-translation with *E. coli* segments *in vivo* and *in vitro*, suggesting the universality of the association with tmRNA and SmpB (*43*). More interestingly, the experiments showed that the C-terminal tail-truncated SmpB with tmRNA can bind to the ribosome, but is inactive for *trans*-translation. This tail-dependent translation suggests the existence of unknown, yet important, roles of the C-terminal tail other than merely associating the tmRNA with the ribosome. Further studies will be required to determine the SmpB functions at various stages.

Our special thanks are due to Mr. Hiroki Ito, of the Life Science Business Group, Hitachi High-Technologies Corp., for his technical assistance and helpful suggestions for the use of the IAsys instrument and the kinetic analyses. We also thank Ms. M. Maeda-Fujii for technical assistance with the RNA preparation, Ms. M. Inoue, Ms. K. Hashimoto and Dr. K. Hosono for cloning and purification of the protein, Dr. A. Takasu for helpful suggestions for the melting profile analyses, and Drs. T. Sakamoto and Y. Muto for valuable advice regarding the NMR analyses. This work was supported by the "Research for the Future" Program (JSPS-RFTF97L00503) from the Japan Society for the Promotion of Science, in part, by Grants-in-Aid for High Technology Research and Scientific Research on Priority Areas from the Ministry of Education, Culture, Sports, Science and Technology (MEXT) of Japan, and by the RIKEN Structural Genomics/Proteomics Initiative (RSGI), the National Project on Protein Structural and Functional Analyses of MEXT.

REFERENCES

1. Gueneau de Novoa, P. and Williams, K.P. (2004) The tmRNA website: reductive evolution of tmRNA in plastids and other endosymbionts. *Nucleic Acids Res.* **32**, D104–D108
2. Zwieb, C., Gorodkin, J., Knudsen, B., Burks, J., and Wower, J. (2003) tmRDB (tmRNA database). *Nucleic Acids Res.* **31**, 446–447
3. Withey, J.H. and Friedman, D.I. (2003) A salvage pathway for protein structures: tmRNA and *trans*-translation. *Annu. Rev. Microbiol.* **57**, 101–123
4. Haebel, P.W., Gutmann, S., and Ban, N. (2004) Dial tm for rescue: tmRNA engages ribosomes stalled on defective mRNAs. *Curr. Opin. Struct. Biol.* **14**, 58–65
5. Yamamoto, Y., Sunohara, T., Jojima, K., Inada, T., and Aiba, H. (2003) SsrA-mediated *trans*-translation plays a role in mRNA quality control by facilitating degradation of truncated mRNAs. *RNA* **9**, 408–418
6. Huang, C., Wolfgang, M.C., Withey, J., Koomey, M., and Friedman, D.I. (2000) Charged tmRNA but not tmRNA-mediated proteolysis is essential for *Neisseria gonorrhoeae* viability. *EMBO J.* **19**, 1098–1107
7. Muto, A., Fujihara, A., Ito, K.I., Matsuno, J., Ushida, C., and Himeno, H. (2000) Requirement of transfer-messenger RNA for the growth of *Bacillus subtilis* under stresses. *Genes Cells* **5**, 627–635
8. Abo, T., Inada, T., Ogawa, K., and Aiba, H. (2000) SsrA-mediated tagging and proteolysis of LacI and its role in the regulation of *lac* operon. *EMBO J.* **19**, 3762–3769
9. Keiler, K.C. and Shapiro, L. (2003) tmRNA is required for correct timing of DNA replication in *Caulobacter crescentus*. *J. Bacteriol.* **185**, 573–580
10. Keiler, K.C. and Shapiro, L. (2003) tmRNA in *Caulobacter crescentus* is cell cycle regulated by temporally controlled transcription and RNA degradation. *J. Bacteriol.* **185**, 1825–1830
11. Karzai, A.W., Susskind, M.M., and Sauer, R.T. (1999) SmpB, a unique RNA-binding protein essential for the peptide-tagging activity of SsrA (tmRNA). *EMBO J.* **18**, 3793–3799
12. Karzai, A.W., Roche, E.D., and Sauer, R.T. (2000) The SsrA-SmpB system for protein tagging, directed degradation and ribosome rescue. *Nat. Struct. Biol.* **7**, 449–455
13. Hanawa-Suetsugu, K., Takagi, M., Inokuchi, H., Himeno, H., and Muto, A. (2002) SmpB functions in various steps of *trans*-translation. *Nucleic Acids Res.* **30**, 1620–1629
14. Karzai, A.W. and Sauer, R.T. (2001) Protein factors associated with the SsrA·SmpB tagging and ribosome rescue complex. *Proc. Natl. Acad. Sci. USA* **98**, 3040–3044
15. Wower, I.K., Zwieb, C.W., Guven, S.A., and Wower, J. (2000) Binding and cross-linking of tmRNA to ribosomal protein S1,

on and off the *Escherichia coli* ribosome. *EMBO J.* **19**, 6612–6621
16. McGinness, K.E. and Sauer, R.T. (2004) Ribosomal protein S1 binds mRNA and tmRNA similarly but plays distinct roles in translation of these molecules. *Proc. Natl Acad. Sci. USA* **101**, 13454–13459
17. Shimizu, Y. and Ueda, T. (2002) The role of SmpB protein in *trans*-translation. *FEBS Lett.* **514**, 74–77
18. Dong, G., Nowakowski, J., and Hoffman, D.W. (2002) Structure of small protein B: the protein component of the tmRNA-SmpB system for ribosome rescue. *EMBO J.* **21**, 1845–1854
19. Someya, T., Nameki, N., Hosoi, H., Suzuki, S., Hatanaka, H., Fujii, M., Terada, T., Shirouzu, M., Inoue, Y., Shibata, T., Kuramitsu, S., Yokoyama, S., and Kawai, G. (2003) Solution structure of a tmRNA-binding protein, SmpB, from *Thermus thermophilus*. *FEBS Lett.* **535**, 94–100
20. Williams, K.P. and Bartel, D.P. (1996) Phylogenetic analysis of tmRNA secondary structure. *RNA* **2**, 1306–1310
21. Felden, B., Himeno, H., Muto, A., McCutcheon, J.P., Atkins, J.F., and Gesteland, R.F. (1997) Probing the structure of the *Escherichia coli* 10Sa RNA (tmRNA). *RNA* **3**, 89–103
22. Zwieb, C., Wower, I., and Wower, J. (1999) Comparative sequence analysis of tmRNA. *Nucleic Acids Res.* **27**, 2063–2071
23. Gutmann, S., Haebel, P.W., Metzinger, L., Sutter, M., Felden, B., and Ban, N. (2003) Crystal structure of the transfer-RNA domain of transfer-messenger RNA in complex with SmpB. *Nature* **424**, 699–703
24. Nameki, N., Chattopadhyay, P., Himeno, H., Muto, A., and Kawai, G. (1999) An NMR and mutational analysis of an RNA pseudoknot of *Escherichia coli* tmRNA involved in *trans*-translation. *Nucleic Acids Res.* **27**, 3667–3675
25. Gill, A., Leatherbarrow, R.J., Hoare, M., Pollard-Knight, D.V., Lowe, P.A., and Fortune, D.H. (1996) Analysis of kinetic data of antibody-antigen interaction from an optical biosensor by exponential curve fitting. *J. Biotech.* **48**, 117–127
26. Delaglio, F., Grzesiek, S., Vuister, G.W., Zhu, G., Pfeifer, J., and Bax, A. (1995) NMRPipe: a multidimensional spectral processing system based on UNIX pipes. *J. Biomol. NMR* **6**, 277–293
27. Goddard, T.D. and Kneller, D.G. SPARKY 3, University of California, San Francisco.
28. Koradi, R., Billeter, M., and Wüthrich, K. (1996) MOLMOL: a program for display and analysis of macromolecular structures. *J. Mol. Graph.* **14**, 51–55
29. Cush, R., Cronin, J.M., Stewart, W.J., Maule, C.H., Molloy, J., and Goddard, N.J. (1993) The resonant mirror: a novel optical biosensor for direct sensing of biomolecular interactions. Part I: Principles of operation and associated instrumentation. *Biosensors & Bioelectronics* **8**, 347–364
30. Canziani, G., Zhang, W., Cines, D., Rux, A., Willis, S., Cohen, G., Eisenberg, R., and Chaiken, I. (1999) Exploring biomolecular recognition using optical biosensors. *Methods* **19**, 253–269
31. Hanawa-Suetsugu, K., Bordeau, V., Himeno, H., Muto, A., and Felden, B. (2001) Importance of the conserved nucleotides around the tRNA-like structure of *Escherichia coli* transfer-messenger RNA for protein tagging. *Nucleic Acids Res.* **29**, 4663–4673
32. Barends, S., Björk, K., Gultyaev, A.P., de Smit, M.H., Pleij, C.W., and Kraal, B. (2002) Functional evidence for D- and T-loop interactions in tmRNA. *FEBS Lett.* **514**, 78–83
33. Zwieb, C., Guven, S.A., Wower, I.K., and Wower, J. (2001) Three-dimensional folding of the tRNA-like domain of *Escherichia coli* tmRNA. *Biochemistry* **40**, 9587–9595
34. Stagg, S.M., Frazer-Abel, A.A., Hagerman, P.J., and Harvey, S.C. (2001) Structural studies of the tRNA domain of tmRNA. *J. Mol. Biol.* **309**, 727–735
35. Gaudin, C., Nonin-Lecomte, S., Tisne, C., Corvaisier, S., Bordeau, V., Dardel, F., and Felden, B. (2003) The tRNA-like domains of *E. coli* and *A. aeolicus* transfer-messenger RNA: structural and functional studies. *J. Mol. Biol.* **331**, 457–471
36. Wower, J., Zwieb, C.W., Hoffman, D.W., and Wower, I.K. (2002) SmpB: a protein that binds to double-stranded segments in tmRNA and tRNA. *Biochemistry* **41**, 8826–8836
37. Felden, B., Hanawa, K., Atkins, J.F., Himeno, H., Muto, A., Gesteland, R.F., McCloskey, J.A., and Crain, P.F. (1998) Presence and location of modified nucleotides in *Escherichia coli* tmRNA: structural mimicry with tRNA acceptor branches. *EMBO J.* **17**, 3188–3196
38. Leulliot, N. and Varani, G. (2001) Current topics in RNA-protein recognition: control of specificity and biological function through induced fit and conformational capture. *Biochemistry* **40**, 7947–7956
39. Williamson, J.R. (2000) Induced fit in RNA-protein recognition. *Nat. Struct. Biol.* **7**, 834–837
40. Valle, M., Gillet, R., Kaur, S., Henne, A., Ramakrishnan, V., and Frank, J. (2003) Visualizing tmRNA entry into a stalled ribosome. *Science* **300**, 127–130
41. Theobald, D.L., Mitton-Fry, R.M., and Wuttke, D.S. (2003) Nucleic acid recognition by OB-fold proteins. *Annu. Rev. Biophys. Biomol. Struct.* **32**, 115–133
42. Draper, D.E. and Reynaldo, L.P. (1999) RNA binding strategies of ribosomal proteins. *Nucleic Acids Res.* **27**, 381–388
43. Jacob, Y., Sharkady, S.M., Bhardwaj, K., Sanda, A., and Williams, K.P. (2005) Function of the SmpB tail in transfer-messenger RNA translation revealed by a nucleus-encoded form. *J. Biol. Chem.* **280**, 5503–5509
44. Bekke, A., Kiefmann, M., Kremerskothen, J., Vornlocher, H.P., Sprinzl, M., and Brosius, J. (1998) The 10Sa RNA gene of *Thermus thermophilus*. *DNA Seq.* **9**, 31–35